

# Disentangling Autoencoders (DAE)

Jaehoon Cha

*Scientific Machine Learning group*

*Rutherford Appleton Laboratory*

*Science and Technology Facilities Council*

United Kingdom

jaehoon.cha@stfc.ac.uk

Jeyan Thiyyagalingam

*Scientific Machine Learning group*

*Rutherford Appleton Laboratory*

*Science and Technology Facilities Council*

United Kingdom

t.jeyan@stfc.ac.uk

**Abstract**—Noting the importance of factorizing or disentangling the latent space, we propose a novel framework for autoencoders based on the principles of symmetry transformations in group-theory, which is a non-probabilistic disentangling autoencoder model. To the best of our knowledge, this is the first model that is aiming to achieve disentanglement based on autoencoders without regularizers. The proposed model is compared to seven state-of-the-art generative models based on autoencoders and evaluated based on reconstruction loss and five metrics quantifying disentanglement losses. The experiment results show that the proposed model can have better disentanglement when variances of each features are different. We believe that this model leads a new field for disentanglement learning based on autoencoders without regularizers.

**Index Terms**—disentanglement, generative models, unsupervised learning, latent representation

## I. INTRODUCTION

Learning generalizable representations of data is one of the fundamental aspects of modern machine learning [Rudin et al.(2022)Rudin, Chen, Chen, Huang, Semenova, and Zhong]. In fact, better representations are more than a luxury now, and is a key to achieve generalization, interpretability, and robustness of machine learning models [Bengio et al.(2013)Bengio, Courville, and Vincent]. One of the primary and desired characteristics of the learned representation is factorizability or disentanglement so that latent representation is composed of multiple, independent generative factors of variations. The disentanglement process renders the latent space features to become independent of one another, and thus provides the basis for novel applications in [Eslami et al.(2018)Eslami, Rezende, Besse, Viola, Morcos, Garnelo, Ruderman, Rusu, Danihelka, Gregor, et al.], [Iten et al.(2020)Iten, Metger, Wilming, Del Rio, and Renner], [Higgins et al.(2021)Higgins, Chang, Langston, Hassabis, Summerfield, Tsao, and Botvinick]. Deep generative models, particularly that build on autoencoders, from the vanilla variational autoencoder (VAE) model [Kingma and Welling(2013)] to various derivatives of VAE, including,  $\beta$ -VAE [Higgins et al.(2017)Higgins, Matthey, Pal, Burgess, Glorot, Botvinick, Mohamed, and Lerchner], [Burgess et al.(2018)Burgess, Higgins, Pal, Matthey, Watters, Desjardins, and Lerchner],  $\beta$ -Total Correlation Variational Autoencoder (TCVAE) [Chen et al.(2018)Chen, Li, Grosse, and Duvenaud], Controlled Capacity Increase-VAE(CCI-VAE) [Burgess et al.(2018)Burgess, Higgins, Pal, Matthey, Watters, Desjardins, and Lerchner], Factor-VAE (FVAE) [Kim and Mnih(2018)], Information Maximizing Variational Autoencoders (InfoVAE) [Zhao et al.(2019)Zhao, Song, and Ermon], and Wasserstein-AE (WAE) [Tolstikhin et al.(2018)Tolstikhin, Bousquet, Gelly, and Schölkopf], have shown to be effective in learning factored representations. The disentangling mechanism, and hence the underpinning functionality of these generative models, rely on two forms of losses: regularization and reconstruction losses [Higgins et al.(2017)Higgins, Matthey, Pal, Burgess, Glorot, Botvinick, Mohamed, and Lerchner], [Chen et al.(2018)Chen, Li, Grosse, and Duvenaud], [Burgess et al.(2018)Burgess, Higgins, Pal, Matthey, Watters, Desjardins, and Lerchner], [Kim and Mnih(2018)], [Tolstikhin et al.(2018)Tolstikhin, Bousquet, Gelly, and Schölkopf]. For instance,  $\beta$ -VAE [Higgins et al.(2017)Higgins, Matthey, Pal, Burgess, Glorot, Botvinick, Mohamed, and Lerchner], which builds on vanilla VAE [Kingma and Welling(2013)], introduces a hyper-parameter  $\beta$  to balance two different types of losses in the VAE, namely, Kullback-Leibler (KL) divergence and reconstruction losses. More specifically, the hyper-parameter  $\beta$  (usually  $> 1$ ) prioritizes the KL-divergence between the learned posterior and prior distributions over reconstruction loss. In Wasserstein-AE [Tolstikhin et al.(2018)Tolstikhin, Bousquet, Gelly, and Schölkopf], hyper-parameter  $\lambda$  is introduced so that the Wasserstein distance between the learned posterior distribution and the prior distribution are improved so that the visual quality of the generated outputs are better than the vanilla VAE.

Although these approaches have advanced the disentangled representation learning, there are a number of issues that limit their full potential. Among these, two of the salient issues that directly conflict with the process of deriving disentangled representations are:

- The tension of balancing two loss components in VAE (and their derivatives) is a delicate and a well-known issue [Asperti and Trentin(2020)]. While the KL-divergence acts as a regularizer by normalizing the smoothness of the latent space (with potential overlapping of latent variables), the reconstruction loss focuses on improving the visual quality of the resulting images. However, the process of

improving reconstruction loss (and hence the visual quality of the output) is oblivious to the shape of the latent space. These contrasting effects render the balancing process more delicate, and when not done correctly, the visual quality of the generated images degrade.

- The notion of known prior distribution is the cornerstone of VAEs and often assumed to be simple isotropic Gaussian distribution. Even with approaches that relax the expressive constrains around the prior exists, such as [Tomczak and Welling(2018)], [Takahashi et al.(2019)Takahashi, Iwata, Yamanaka, Yamada, and Yagi], the presence of prior (even if optimal) can easily create a tension between the true distribution and the prior. Hence, this can exert an additional pressure on latent space regularization, particularly if the distribution of the real data does not match the prior.

In this paper, we propose a novel autoencoder-based generative approach for deriving disentangled representations while addressing the concerns highlighted above. More specifically, the proposed approach, which we name as Disentangling Auto-Encoder (DAE), relies on the concept symmetry transformation [Higgins et al.(2018a)Higgins, Amos, Pfau, Racaniere, Matthey, Rezende, and Lerchner], which is often formalized using group theory. By carefully deriving a set of symmetry transformations on the latent space for each latent variables, we achieve a powerful method for obtaining disentangled representations. The proposed model has the following advantages over conventional VAE-based approaches:

- 1 It is a non-probabilistic, group theory-based approach. As such, neither there is any assumption of any priors nor the process of learning any posteriors from the input data; and
- 2 As a consequence of (1), the proposed approach fully eliminates the need for any distribution regularization mechanism (such as KL-divergence) in the latent space, and thus the approach renders a model that can fully focus on reconstruction loss for improving the visual quality of the generated outputs.

Our exhaustive evaluation, covering seven state-of-the-art autoencoder-based models across five different disentangling metric, shows that the proposed model has a powerful disentangling ability while offering remarkable visual quality. This is particularly true when the variances of each feature are different, a common observation across all real datasets.

The rest of this paper is organized as follows. In Section II we provide a necessary theoretical background and review the related work, particularly focusing on autoencoder-based approaches due to its nature of strongly principled yet simplistic approach to generative modeling. This is then followed by a derivation of autoencoder-based, structure preserving framework in Section III. In Section IV, we exhaustively evaluate the proposed method against a number of relevant models with a number of hyperparameters and toy examples, and discuss our findings. We then conclude the paper in Section V with directions for further research.

## II. RELATED WORK

### A. Disentanglement

Disentangled representation learning [Bengio et al.(2013)Bengio, Courville, and Vincent], [Higgins et al.(2018a)Higgins, Amos, Pfau, Racaniere, Matthey, Rezende, and Lerchner] focuses disentangling any correlations between these latent variables, such that their variations are orthogonal with each other. Decoupling any correlations between latent variables matches single underlying factor with one component of latent variables and can serve a number of downstream applications including the improvement of predictive performance [Locatello et al.(2019)Locatello, Tschannen, Bauer, Rätsch, Schölkopf, and Bachem], effective learning with a small number of samples [Van Steenkiste et al.(2019)Van Steenkiste, Locatello, Schmidhuber, and Bachem], [Yue et al.(2021)Yue, Wang, Sun, Hua, and Zhang], discovery of physical concepts [Iten et al.(2020)Iten, Metger, Wilming, Del Rio, and Renner] and enabling 3D shape reconstruction from 2D images [Pan et al.(2020)Pan, Dai, Liu, Loy, and Luo].

A large body of can be found around disentanglement, and ideal properties of disentangled representation can be found in [Ridgeway(2016)], [Eastwood and Williams(2018)], [Ridgeway and Mozer(2018)], [Zaidi et al.(2020)Zaidi, Boilard, Gagnon, and Carbonneau]. Among different desirable properties of disentanglement, three are critically important, namely, modularity, compactness and explicitness. The modularity property focusses on the effect of one learnt factor on others, or in other words, independence. The compactness property measures how effectively one learnt factor covers the representation. The explicitness property measures the relationship between the learned factors and true factors of data. A number of metrics have been proposed in the literature to quantify these properties [Higgins et al.(2017)Higgins, Matthey, Pal, Burgess, Glorot, Botvinick, Mohamed, and Lerchner], [Kim and Mnih(2018)], [Eastwood and Williams(2018)], [Chen et al.(2018)Chen, Li, Grosse, and Duvenaud], [Do and Tran(2019)], [Sepliarskaia et al.(2019)Sepliarskaia, Kiseleva, de Rijke, et al.]. In our work, we use the notions outlined in [Zaidi et al.(2020)Zaidi, Boilard, Gagnon, and Carbonneau], where the metrics are divided into three classes, namely, Intervention-based metrics, Predictor-based metrics, and Information-based metrics. These metrics can be of indicators to quantify modularity, compactness, explicitness robustness to noise, nonlinear relationships between learnt factors and true factors.

### B. Probabilistic Generative Models based on Autoencoder Model

Autoencoder (AE), which consists of an encoder  $E_\phi$  that maps an observations space to a lower-dimensional latent space, and a decoder  $D_\theta$  that re-maps the latent space to the observation space, effectively learn meaningful representations in the latent space by minimizing the reconstruction loss,  $\mathcal{L}_{recon}$  (cross-entropy or  $L_2$ ).

Probabilistic generative models based on AE are achieved by replacing the conventional encoder and decoder with

probabilistic variants of them [Kingma and Welling(2013)], [Rezende and Mohamed(2015)], [Higgins et al.(2017)Higgins, Matthey, Pal, Burgess, Glorot, Botvinick, Mohamed, and Lerchner], [Tolstikhin et al.(2018)Tolstikhin, Bousquet, Gelly, and Schölkopf], respectively. Given an observation  $\mathbf{x} \in \mathbb{R}^n$ , the VAE [Kingma and Welling(2013)]-based approaches rely on the variational theory. They use the probabilistic encoder, denoted by  $q_\phi(\mathbf{z}|\mathbf{x})$ , to approximate the intractable true posterior and the probabilistic decoder, denoted by  $p_\theta(\mathbf{x}|\mathbf{z})$  that reconstructs the  $\mathbf{x}$  from  $\mathbf{z}$ . In an ideal world, the resulting posterior  $q_\phi(\mathbf{z}|\mathbf{x})$  should match well with the prior distribution  $p(\mathbf{z})$ . However, this is rarely the case, and weights in the encoder and decoder are trained accounting this fact by relying on a loss function that measures not only the reconstruction loss, but also the similarity of the posterior and prior distributions. The similarity between two different distributions is, usually, computed using the KL-divergence, but alternative techniques can be used [Tolstikhin et al.(2018)Tolstikhin, Bousquet, Gelly, and Schölkopf]. The combined loss is referred to as the Evidence Lower Bound (ELBO) [Kingma and Welling(2013)], and defined as follows,

$$\begin{aligned} \mathcal{L}_{VAE}(\phi, \theta) = \\ \mathbb{E}_{\mathbf{z} \sim q_\phi(\mathbf{z}|\mathbf{x})} [\log p_\theta(\mathbf{x}|\mathbf{z})] + KL(q_\phi(\mathbf{z}|\mathbf{x})||p(\mathbf{z})) \leq \log p(\mathbf{x}) \end{aligned} \quad (1)$$

The first term in (1) can be estimated from samples  $\mathbf{z}$  drawn from the approximate posterior  $q_\phi(\mathbf{z}|\mathbf{x})$  using reparameterization trick [Kingma and Welling(2013)]. The second term plays a crucial role as a regularizer to minimize  $q_\phi(\mathbf{z}|\mathbf{x})$  and  $p(\mathbf{z})$ .

Majority of the previous work on disentangled representation learning are predominantly based on probabilistic models, particularly builds on VAE. They enforce regularization in the latent space that either regularizes the approximate posterior  $q_\phi(\mathbf{z}|\mathbf{x})$  or the aggregate posterior  $p(\mathbf{z})$ , as summarized in [Tschannen et al.(2018)Tschannen, Bachem, and Lucic]. The overall objective of majority of the VAE-based methods can be expressed as:

$$\mathcal{L}_{recon}(\phi, \theta) + \eta \mathcal{L}_{reg}(\phi) \quad (2)$$

where  $\mathcal{L}_{reg}(\phi)$  is a regularizer of a generative model and  $\eta$  is a hyperparameter to balance between two losses. In the experiments, we compare the proposed model with vanilla VAE,  $\beta$ -VAE,  $\beta$ -TCVAE, CCI-VAE, FVAE, InfoVAE and WAE. For convenience, we summarize all these models in Table I.

Depending on the selection of regularizers, these models deliver different disentangling capabilities. Furthermore, in all these models, a regularizer drives the  $\mathcal{L}_{VAE}$  towards a larger bound on the marginal log-likelihood term to ensure better KL-loss. This, naturally, results in lower quality outputs. In contrast, the method we propose here is not a probabilistic model, and thus, does not rely on variational inference or any approximation of posteriors or assumption of priors, totally eliminating the need for any regularizers. Instead, the proposed model relies on a deterministic AE model for deriving the latent space, which is then manipulated very carefully to derive the disentangled latent factors while providing the true generative capability to AEs. In the absence of any regularizers, the

proposed model purely focuses on the reconstruction loss while achieving perfect disentangled representations, as we shall see in Section IV.

### III. FRAMEWORK FOR DAE

Here we establish the connection between autoencoder and disentangled representation in the context of group theory, define the mathematical framework and corresponding neural network-based architecture underpinning the proposed disentangling autoencoder. We also provide a background around disentangled representations.

#### A. Disentangled representation

The notion of disentangled representation is mathematically defined using the concept of symmetry in [Higgins et al.(2018a)Higgins, Amos, Pfau, Racaniere, Matthey, Rezende, and Lerchner]. For example, horizontal and vertical translations are symmetry transformations in two-dimensional grid and actions of the transformations change the location of an object in this two-dimensional grid. For the disentanglement, one need to find subgroups of a symmetry group which independently act on subspaces of a latent space. If actions by transformations of each subgroup only affect the corresponding subspace, the actions are called *disentangled group actions*. In other words, disentangled group actions only change a specific property of the state of an object, and leaves other properties invariant. If there is a transformation in a vector space of representations, corresponding to a disentangled group action, the representation is called a *disentangled representation*. A detailed coverage of these aspects can be found in [Higgins et al.(2018a)Higgins, Amos, Pfau, Racaniere, Matthey, Rezende, and Lerchner].

**Definition III.1.** [Higgins et al.(2018a)Higgins, Amos, Pfau, Racaniere, Matthey, Rezende, and Lerchner] Suppose that we have a group action  $\cdot : G \times X \rightarrow X$ , and the group  $G$  decomposes as a direct product  $G = G_1 \times \dots \times G_n$ . Let the action of the full group, and the actions of each subgroups be referred to as  $\cdot$  and  $\cdot_i$ , respectively. Then, the action is disentangled if there is a decomposition  $X = X_1 \times \dots \times X_n$ , and actions  $\cdot_i : G_i \times X_i \rightarrow X_i$ ,  $i \in \{1, \dots, n\}$  such that:

$$(g_1, \dots, g_n) \cdot (\mathbf{x}_1, \dots, \mathbf{x}_n) = (g_1 \cdot \mathbf{x}_1, \dots, g_n \cdot \mathbf{x}_n) \quad (3)$$

for all  $g_i \in G_i$  and  $\mathbf{x}_i \in X_i$ .

Let  $W$  be the set of world-states. Suppose there is a generative process  $b : W \rightarrow O$  leading from world-states to observations,  $O$ , and an inference process  $h : O \rightarrow Z$  leading from observations to an agent's representations,  $Z$ . Consider the composition  $f : W \rightarrow Z$ ,  $f = h \circ b$ . Supposed also that there is a group  $G$  of symmetries acting on  $W$  via an action  $\cdot : G \times W \rightarrow W$ . The goal is to find a corresponding action  $\cdot : G \times Z \rightarrow Z$  so that the symmetry structure of  $W$  is reflected in  $Z$ . In other words, an action on  $Z$  corresponding to the action on  $W$  is desirable. This can be achieved if the following condition is satisfied:

TABLE I  
COMPARISON OF DIFFERENT VAE-BASED MODELS W.R.T THE REGULARIZERS THEY EMPLOY.

Model	$L_{reg}(\phi)$	Notes
VAE	$KL(q_\phi(\mathbf{z} \mathbf{x}), q(\mathbf{z}))$	
$\beta$ -VAE	$\beta KL(q_\phi(\mathbf{z} \mathbf{x}), q(\mathbf{z}))$	Usually, $\beta$ is greater than 1
$\beta$ -TCVAE	$I(\mathbf{z}, \mathbf{x}) + \beta KL(q_\phi(\mathbf{z} \mathbf{x}), \prod_j q_\phi(\mathbf{z}_j \mathbf{x})) + \sum_j KL(q_\phi(\mathbf{z}_j \mathbf{x}), q(\mathbf{z}_j))$	$I(\cdot, \cdot)$ is a mutual information
CCI-VAE	$\beta \ KL(q_\phi(\mathbf{z} \mathbf{x}), q(\mathbf{z})) - C\ $	$C$ is a capacity
FVAE	$KL(q_\phi(\mathbf{z} \mathbf{x}), q(\mathbf{z})) + \gamma KL(q_\phi(\mathbf{z} \mathbf{x}), z')$	$z'$ is random permutation of $z \sim q_\phi(\mathbf{z} \mathbf{x})$
InfoVAE	$KL(q_\phi(\mathbf{z} \mathbf{x}), q(\mathbf{z})) + \lambda MMD(q_\phi(\mathbf{z} \mathbf{x}), q(\mathbf{z}))$	$MMD(\cdot, \cdot)$ is Maximum Mean Discrepancy
WAE	$\lambda MMD(q_\phi(\mathbf{z} \mathbf{x}), q(\mathbf{z}))$	

$$g \cdot f(\mathbf{w}) = f(g \cdot \mathbf{w}) \quad \forall g \in G, \mathbf{w} \in W. \quad (4)$$

In other words, the action,  $\cdot$ , should commute with  $f$ , which adheres to the definition of the equivariant map. Hence,  $f$  is an equivariant map.

$$\begin{array}{ccc} G \times W & \xrightarrow{\cdot^W} & W \\ id_G \times f \downarrow & & \downarrow f \\ G \times Z & \xrightarrow{\cdot^Z} & Z \end{array}$$

From [Higgins et al.(2018a) Higgins, Amos, Pfau, Racaniere, Matthey, Rezende, and Lerchner], a disentangled representation can be defined as follows:

**Definition III.2.** [Higgins et al.(2018a) Higgins, Amos, Pfau, Racaniere, Matthey, Rezende, and Lerchner] The representation  $Z$  is disentangled with respect to  $G = G_1 \times \dots \times G_n$  if

1. There is an action  $\cdot : G \times Z \rightarrow Z$ ,
2. The map  $f : W \rightarrow Z$  is equivariant between the actions on  $W$  and  $Z$ , and
3. There is a decomposition  $Z = Z_1 \times \dots \times Z_n$  or  $Z = Z_1 \bigoplus \dots \bigoplus Z_n$  such that each  $Z_i$  is fixed by the action of all  $G_j$ ,  $j \neq i$  and affected only by  $G_i$ .

### B. Association between the Disentangled Representation and Autoencoder

With the definition of equivariant map in place, the overarching goal of finding a disentangled representation is equivalent to finding  $f$  that satisfies (4). However, in general, one cannot control the generative process of the nature. In addition, without loss of generality, we can easily assume the generative process  $b$  is an equivariant map. In other words, action on the set of world-states commute with  $b$ ,

$$g \cdot b(\mathbf{w}) = b(g \cdot \mathbf{w}) \quad \forall g \in G, \mathbf{w} \in W. \quad (5)$$

Now, consider the inference process  $h$ , defined above.

**Theorem III.3.** Suppose a generative process  $b$  is an equivariant map satisfying (5). Then, there exists a function  $f$  that satisfies (4) if an inference process  $h : O \rightarrow Z$  is an equivariant map satisfying,

$$g \cdot h(\mathbf{o}) = h(g \cdot \mathbf{o}) \quad \forall g \in G, \mathbf{o} \in O. \quad (6)$$

*Proof.* Suppose that there  $b$  satisfies (5) and  $h$  is an equivariant map. Then

$$g \cdot f(\mathbf{w}) = g \cdot h(b(\mathbf{w})) \quad (7)$$

$$= h(g \cdot b(\mathbf{w})) \quad (8)$$

$$= h(b(g \cdot \mathbf{w})) \quad (9)$$

$$= f(g \cdot \mathbf{w})) \quad (10)$$

□

$$\forall g \in G, \mathbf{w} \in W.$$

Following the Theorem III.3, the goal of disentangling is same as finding an inference process  $h : O \rightarrow Z$ . Although there is no guarantee that one can find a compatible action  $\cdot : G \times Z \rightarrow Z$  satisfying (6), if  $h$  is bijective then (6) can be expressed as follows,

$$g \cdot z = h(g \cdot h^{-1}(z)) \quad (12)$$

This equivariant map can be learnt by autoencoders. Let  $h$  and  $h^{-1}$  be an encoder,  $E_\phi$ , and a decoder,  $D_\theta$ , of an autoencoder. Then, the group action  $\cdot : G \times Z \rightarrow Z$  can be defined by

$$G \times Z \xrightarrow{id_G \times D_\theta} G \times O \xrightarrow{\cdot^O} O \xrightarrow{E_\phi} Z$$

### C. Towards Disentangling Autoencoder

Consider a grid world example outlined in [Higgins et al.(2018a) Higgins, Amos, Pfau, Racaniere, Matthey, Rezende, and Lerchner], where a circle with different gray scales can be moved horizontally and vertically (in other words, the features are positions and colour). Here, horizontal and vertical translations and colour changes are, in fact, symmetry transformations, as since none of these transformations affect the identity of the object, namely, circle. Let  $N_x$ ,  $N_y$  and  $N_c$ , be the possible number of horizontal and vertical positions and gray levels. In [Higgins et al.(2018a) Higgins, Amos, Pfau, Racaniere, Matthey, Rezende, and Lerchner], a natural equivariant map  $f : W \rightarrow Z$  is defined as:

$$f(x, y, c) = (e^{2\pi ix/N_x}, e^{2\pi iy/N_y}, e^{2\pi ic/N_c}). \quad (13)$$

Although this identifies that this mapping is indeed a disentangling group representation, it does not provide a method for realising this mapping to be of practical utility, particularly in the AE setting. In this paper, we show that this can be achieved in the context of AE by three layers, namely, normalisation, interpolation and Euler layers.

However, in our case, the number of possible elements in the subgroups (such as  $N_x, N_y$  or  $N_c$ ) are not known a priori, and in fact, cannot be extracted either without access to the ground truth. However, it is possible to estimate the relative ratio of these possible elements in the subgroups, using techniques like principal component analysis (PCA) [] or similar. Let this relative ratio of possible number of elements in the subgroups be denoted by a hyper-parameter  $W$ . Given that representations  $Z$  are to be derived from observations  $O$ , the goal is to find an encoder  $f : O \rightarrow Z$  such that  $\forall o \in O$

$$f(o) = (e^{i\theta_1}, \dots, e^{i\theta_n}). \quad (14)$$

where  $n$  is the number of subgroups.

#### D. Architecture of the DAE

In mapping our theory to an architecture, the disentangling process maps the observation space  $O$  to a factorized latent space  $Z$ . In doing so, we make the following key realistic requirements when disentangling the latent space:

- 1) Ideally, a one-to-one mapping between the observation and its corresponding representation in the latent space is desired,
- 2) Variance of each feature varies depending on possible number of elements, and
- 3) Elements in each feature are equally likely/distributed.

We address each of these requirements using three different layers, which have been mentioned above, interposed between the encoder and decoder otherwise a conventional AE model. This is illustrated in Figure 1, and we describe each of these layers below in detail.

#### E. Batch min-max normalisation and Euler Layer

With  $e^{2\pi i\theta} = \cos(2\pi\theta) + i\sin(2\pi\theta)$ , we use Euler layer to map the outputs of the encoder  $z = (z_1, z_2, \dots, z_n)$  to  $(\cos(2\pi z_1), \sin(2\pi z_1), \dots, \cos(2\pi z_n), \sin(2\pi z_n))$  as described in III-C. Since a map  $\theta \rightarrow e^{2\pi i\theta}$  makes isomorphism between  $\mathbb{R}/\mathbb{Z}$ , if the inputs of the Euler layer are within  $[0, 1]$ , then the map  $z_k \rightarrow e^{2\pi i z_k}$  is bijective. In order to ensure the inputs of the Euler layer are within  $[0, 1]$ , we apply batch min-max normalisation to the outputs of the encoder. This layer uses the batch minimum and the maximum of each component of the encoder output during training. As minimum and maximum values vary from batch (mini-batch) to batch (mini-batch), we update the moving minimum and maximum values during the training process, and use them during the test phase, akin to a batch normalization layer [Ioffe and Szegedy(2015)]. In order to slowly learn the moving minimum and maximum values, they are initialized close to the middle point of  $[0, 1]$ . Finally, we need to multiply  $W = (N_1, N_2, \dots, N_n)$  to the output of

the batch min-max normalisation layer to consider the different number of possible elements at different features. In order to find  $W$  that describes the possible number of elements for each feature in the latent space better, we calculate singular values by PCA. Then, we divide all singular values with its max values and round to one decimal place. The values smaller than unity are replaced with hyper-parameter  $\alpha$  and it becomes  $W$ . The relevant algorithm is shown in Algorithm 1 in the supplementary material.

#### F. Interpolating Layer

Mapping the outputs of the encoder  $Enc$  to  $e^{2\pi i z}$  helps achieving natural equivariant map from the observation space to the latent space. However, two key issues remain: firstly, having the ability to provide a reasonable coverage of the latent values to ensure high quality generative process, and secondly, ability to break the fully predictable and deterministic nature of AE model. These two issues are addressed by this layer, where two operations are performed: One is that missing values are interpolated, and secondly, a zero-mean, unit variance, weight-sensitive Gaussian noise is added to the outputs of the stretching layer so that nearly all possible values in a unit circle are observed during training. The relevant algorithm is shown in Algorithm 2 in the supplementary material. It is worth noting that this layer will not be used during the inference / test phase.

## IV. EVALUATION AND RESULTS

We performed our evaluation on the basis of different models being able to disentangle the latent space. We cover our methodology, particularly around datasets, baseline models and relevant performance metrics below.

#### A. Datasets

One of the critical challenges around evaluating disentanglement is identifying suitable datasets. It is difficult to identify a universal dataset that can be used to study this problem. In the literature, different datasets have been used for different purposes. For example, dSprite [Matthey et al.(2017)Matthey, Higgins, Hassabis, and Lerchner] dataset has been used in  $\beta$ -VAE,  $\beta$ -TCVAE, CCI-VAE and FVAE. Although this dataset is useful to understand the traversal order of the latent space, the lack of possibility to fully disentangle the feature space of this dataset prevents us from using this for our study. Similarly, majority of the datasets, such as 3D Chair [Burgess and Kim(2018)] and CelebA [Liu et al.(2015)Liu, Luo, Wang, and Tang] lack the ground truth enabling us to quantify the disentanglement. Therefore, in this paper, we utilise the dataset that has been first utilised in [Higgins et al.(2018b)Higgins, Amos, Pfau, Racaniere, Matthey, Rezende, and Lerchner], with relevant enhancements, which we describe below. These enhancements are essential to account for the variations we outlined in our work. The datasets are:

- 1) Dataset with pure positional features( $XY$ ): This dataset consist of circles with variations to their  $x$  and  $y$  positions. This is a rather small, but very effective, dataset consisting of a circles of radius 15 units in a  $84 \times 84$

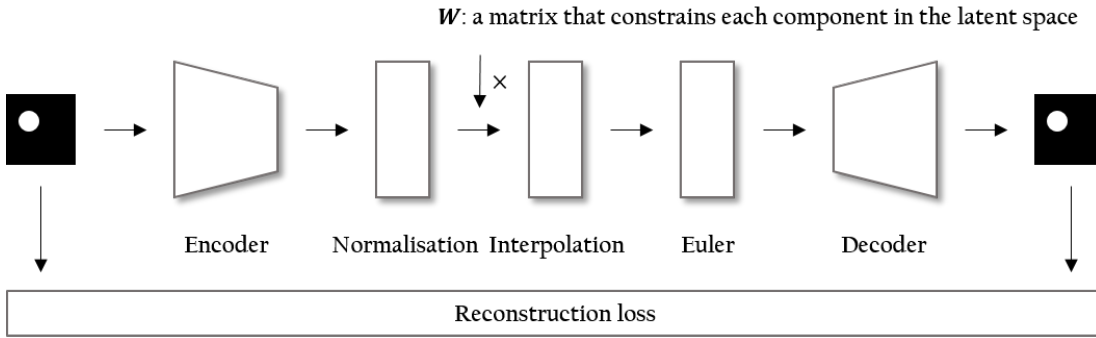


Fig. 1. Illustration of the DAE architecture.

frame translated on the  $XY$  plane, so that there are 53 unique  $X$  positions and 53 unique  $Y$  positions. Albeit being a small, this dataset is effective enough to test the disentanglement. A perfect disentanglement should be a rectangular shape of circles, only with linear variations.

- 2) Dataset with positional and colour features ( $XYC$ ): This is the same as the  $XY$  dataset, but with colour information (more specifically, the brightness) is added to the circle. This dataset is used as an example of disentanglement in [Higgins et al.(2018a) Higgins, Amos, Pfau, Racaniere, Matthey, Rezende, and Lerchner].
- 3) Dataset with positional and shape features ( $YS$ ): This dataset has three features: positional information  $x, y$  and shape  $S$ , which is either a circle, rectangle or a diamond. While shape can have three different options,  $x$  and  $y$  positions can have 53 options.
- 4) Dataset with positional, colour and shape features ( $YCS$ ) : This dataset is similar to the  $YS$  dataset but with colour feature added.
- 5) 3D-Shape Dataset [Burgess and Kim(2018)]: This dataset has 480,000, three- channel RGB,  $64 \times 64 \times 3$  images of 3D-shapes with ground truth factors of four shapes, eight scales, 15 orientations, 10 floor colour, 10 wall colours, and 10 object colours. With the lack of space, results for this dataset can be found in the supplementary material.
- 6) 3D Face Model Dataset [Paysan et al.(2009) Paysan, Knothe, Amberg, Romdhani, and Vetter]: This dataset has 127050 ,gray-scale,  $64 \times 64$  images of 3D face with ground truth factors of 50 different face id, 21 azimuth, 11 elevation and 11 lighting. With the lack of space, results for this dataset can be found in the supplementary material.

## B. Baseline Models

We considered seven different baselines for evaluation, namely, VAE,  $\beta$ -VAE,  $\beta$ -TCVAE, CCI-VAE, FVAE, InfoVAE and WAE. As the proposed technique is purely the AE-based method, we have not included any GAN-specific baselines. To render a fair evaluation mechanism, we used the same encoder and decoder architectures, and same latent space dimensions (for each baseline) throughout the evaluation. We provide a

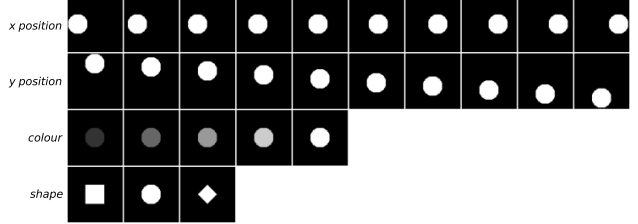


Fig. 2. Four elements in datasets.  $x$  and  $y$  positions have 53 elements, colour has 5 elements and shape has 3 elements.

detailed description of these, including the details of the system on which these evaluations were carried out as part of the supplementary material.

## C. Performance Metrics

As outlined in Section II-A, there are a number of metrics that can be used to study the performance of disentanglement, depending on the nature of the dataset, access to ground truth, availability of latent factors, and the number of dimensions in the latent space. We use the following metrics: **(a) Visualization of the latent space:** We show all pairs of two components of the latent space when using  $XY$  and  $YCS$  datasets to show the orthogonality of each pair of two components, and to verify the models can still disentangle the positional features when colour and shape features, which have relatively small number of elements, are added to the dataset. **(b) Numerical disentanglement score:** The five disentanglement scores are chosen from each of the disentanglement metric classes (see Section II-A), namely,  $z$ -diff and  $z$ -min from the intervention-based,  $dei$ -rf from the predictor-based, and  $jemmig$  and  $dcimig$  from the information-based metric classes.

## D. Hyper-parameter Setting

The proposed model relies on an easily determinable hyper-parameter, namely,  $W$ , that captures the relative ratio of the number of elements for each feature. As shall we discussed later, although the proposed model is not heavily sensitive to this hyper-parameter, providing sensible values to this hyper-parameter can lead to best outcomes. Each of the dataset we are using for the evaluation of the work has varying number

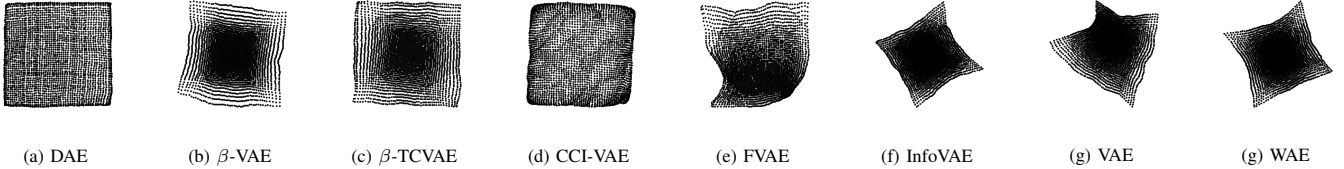


Fig. 3. Positional relationships (X-Y) in the latent space learned by different models when a dataset has only  $x$  and  $y$  positional features. In this case, most models are able to disentangle  $x$  and  $y$  positional features in the latent space.

TABLE II  
 $\bar{S}$  VALUES FOR DIFFERENT DATASETS

Dataset	$\bar{S}$
XY	[1.0, 1.0]
XYC	[1.0, 1.0, 0.8]
XYS	[1.0, 1.0, 0.8]
XYCS	[1.0, 1.0, 0.8, 0.8]
3D-Shape	[1.0, 1.0, 1.0, 1.0, 0.5, 0.5]

TABLE III  
BEST HYPER-PARAMETERS FOR MODELS FOR DIFFERENT DATASETS.

Model / Dataset	XY	XYC	XYS	XYCS	3D-Shape
DAE ( $\alpha$ )	—	0.005	0.001	0.0005	0.005
$\beta$ -VAE ( $\beta$ )	16	64	64	32	64
$\beta$ -TCVAE ( $\beta$ )	32	64	128	128	32
CCI-VAE (C)	500	100	100	100	100
FVAE ( $\gamma$ )	200	100	100	500	5
InfoVAE ( $\lambda$ )	100	100	100	500	100
WAE ( $\lambda$ )	1	50	30	50	50

of features, and hence the variance between these components. As stated before, we used Algorithm 1 obtain the values for this hyper-parameter, which is underpinned by PCA (in our case), and the typical values for  $\bar{S}$  in Algorithm 1 are shown in Table II.

### E. Results and Discussions

Accounting the limitations of space, we present the results of top scores with respect to hyperparameters. All results can be found as part of the supplementary material.

1) *Visualization of the Latent Space*: We first show the disentangled (two-dimensional) latent space for the  $XY$  dataset in Figure 3 along with the relevant hyperparameters in Table III. As  $x$  and  $y$  positions collectively have 53 possible elements, the notion of hyper-parameter for this setting is irrelevant, and thus  $\bar{S} = [1.0, 1.0]$ . As can be seen, the proposed model, in general, provides the ideal grid-shape outlined in [Higgins et al.(2018a)Higgins, Amos, Pfau, Racaniere, Matthey, Rezende, and Lerchner]. The plain vanilla VAE model offer the worst performance. Other models, such as  $\beta$ -VAE,  $\beta$ -TCVAE and CCI-VAE models also comes closer to the ideal pattern, and thus most models are able to disentangle  $x$  and  $y$  positions.

However, when colour or shape feature is added to this  $x - y$  dataset (i.e., for  $XYC$ ,  $XYS$  and  $XYCS$  datasets), the disentanglement can become a significant challenge, other than

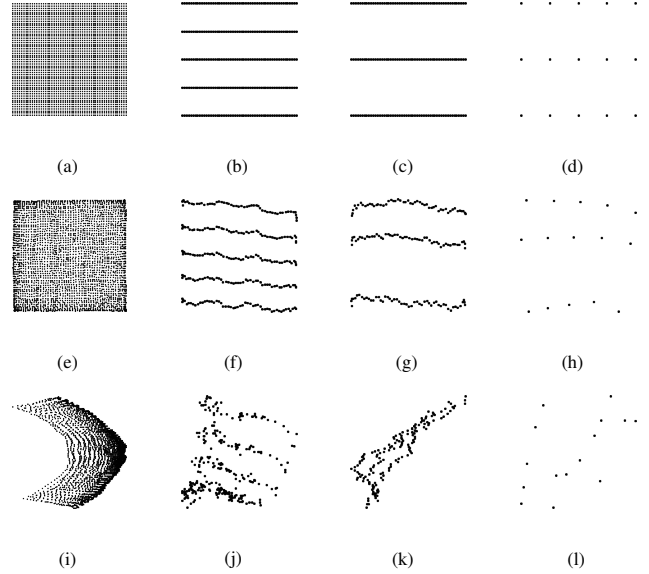


Fig. 4. Relationships between  $x-y$ ,  $x-c$ ,  $x-s$  and  $c-s$  features in each column, respectively. The first and second rows show the ideal relationships in the latent space. The second and third rows show the learned latent variables for the DAE and CCI-VAE models.

for the proposed model. We show this in Figure 4. For  $XYCS$  dataset, since  $\bar{S} = [1.0, 1.0, 0.8, 0.8]$ , we evaluate the proposed model with a hyper-parameter  $W = [1.0, 1.0, \alpha, \alpha]$ . For the reasons of brevity, we present the ideal  $x - y$ ,  $x - c$ ,  $x - s$ , and  $c - s$  relationships and the relationships learned by top two models based on disentanglement scores. These are from the proposed and CCI-VAE models. As we can see, The learned latent space using the proposed model is almost same as the ideal case. However, CCI-VAE fails to ideally disentangle the  $x - y$  positions when colours and shape features are added. In addition to these pairs of latent space, reconstructions of latent traversals across each latent dimension are shown in Figure 14 as part of the supplementary materials along with the latent spaces for the other models.

2) *Disentanglement Scores*: We present the disentanglement scores for  $XY$ ,  $XYC$ ,  $XYS$  and  $XYCS$  datasets in Tables IV, VI, VII and V, respectively. Again, for the reasons of brevity, we present the best scores for each model with relevant hyper-parameter settings in  $XY$  and  $XYCS$  datasets. Full set of results can be found in the Supplementary section.

From these results, we make the following key observations for each of the datasets, and metrics:

TABLE IV  
DISENTANGLEMENT SCORES FOR THE *XY* DATASET

Models / Metrics	z-diff	z-var	dci-rf	jemmig	dcimig
DAE	<b>1.00</b>	<b>1.00</b>	<b>0.99</b>	<b>0.85</b>	<b>0.84</b>
VAE	<b>1.00</b>	0.84	0.23	0.38	0.25
$\beta$ -VAE	<b>1.00</b>	<b>1.00</b>	0.91	0.63	0.60
$\beta$ -TCVAE	<b>1.00</b>	<b>1.00</b>	0.93	0.69	0.68
CCI-VAE	<b>1.00</b>	<b>1.00</b>	0.97	0.82	0.81
FVAE	<b>1.00</b>	<b>1.00</b>	0.94	0.68	0.65
InfoVAE	<b>1.00</b>	<b>1.00</b>	0.20	0.34	0.20
WAE	<b>1.00</b>	<b>1.00</b>	0.58	0.51	0.43

TABLE V  
DISENTANGLEMENT SCORES FOR THE *XYCS* DATASET

Models / Metrics	z-diff	z-var	dci-rf	jemmig	dcimig
DAE	<b>1.00</b>	<b>1.00</b>	<b>0.95</b>	<b>0.83</b>	<b>0.84</b>
VAE	0.82	0.24	0.08	0.27	0.09
$\beta$ -VAE	0.97	0.89	0.51	0.40	0.37
$\beta$ -TCVAE	<b>1.00</b>	0.73	0.55	0.50	0.52
CCI-VAE	<b>1.00</b>	0.99	0.62	0.48	0.41
FVAE	0.99	0.92	0.19	0.27	0.15
InfoVAE	0.90	0.50	0.21	0.31	0.13
WAE	0.83	0.58	0.20	0.27	0.13

- 1) DAE model outperforms all models across all metrics in *XY*, *XYC*, *XYs*, and *XYCS* datasets.
- 2) The dic-rf, jemmig and dcimig scores of FVAE drop when either colour or shape feature is added to the *XY* dataset.
- 3)  $\beta$ -VAE,  $\beta$ -TCVAE and CCI-VAE show relatively better performance than the other models, yet, their dci-rf, jemmig and dcimig scores are reducing as colour and shape features are added.
- 4) From Figures 15-18, we can notice that the proposed model keeps the reconstruction loss small while increasing disentanglement scores. On the other hand, the reconstruction loss of  $\beta$ -VAE,  $\beta$ -TCVAE and CCI-VAE are increasing when their disentanglement scores are increasing.

## V. CONCLUSIONS

In the context of representation learning, being able to factorize or disentangle the latent space dimensions is crucial for obtaining latent representations that is composed of multiple, independent generative factors of variations. On this aspect, deep generative models, particularly that build on autoencoders, play an important role. AE-, particularly, VAE-based models employ two forms of losses to balance the two conflicting goals representation learning: reconstruction loss and factorizability. To favour one over the other, many factorizing models rely on one or more hyperparameters which increases disentanglement ability while reducing reconstruction ability.

In this paper, we presented a non-probabilistic, disentangling autoencoder model, namely, DAE, to address this problem. By exploiting the principles of symmetry transformations in group-

theory, we presented a model that only has a reconstruction loss. Although the model relies on a hyper-parameter, the model is not overly sensitive to this, and the value can easily be obtained using PCA-like technique. Our evaluation, performed against a number of VAE-based models, using a number of metrics shows that our model can offer the best performance on a number of datasets.

Although the results are encouraging, a number of aspects remain to be investigated. We intend to investigate a number of issues, including evaluation against other metrics and public datasets, and automatic determination of an optimal value for the hyper-parameter.

## REFERENCES

[Asperti and Trentin(2020)] Andrea Asperti and Matteo Trentin. Balancing reconstruction error and kullback-leibler divergence in variational autoencoders. *IEEE Access*, 8:199440–199448, 2020.

[Bengio et al.(2013)] Bengio, Courville, and Vincent] Yoshua Bengio, Aaron Courville, and Pascal Vincent. Representation learning: A review and new perspectives. *IEEE transactions on pattern analysis and machine intelligence*, 35(8):1798–1828, 2013.

[Burgess and Kim(2018)] Chris Burgess and Hyunjik Kim. 3d shapes dataset. <https://github.com/deepmind/3dshapes-dataset/>, 2018.

[Burgess et al.(2018)] Burgess, Higgins, Pal, Matthey, Watters, Desjardins, and Lerchner] Christopher P Burgess, Irina Higgins, Arka Pal, Loic Matthey, Nick Watters, Guillaume Desjardins, and Alexander Lerchner. Understanding disentangling in  $\beta$ -vae. *arXiv preprint arXiv:1804.03599*, 2018.

[Chen et al.(2018)] Chen, Li, Grosse, and Duvenaud] Ricky TQ Chen, Xuechen Li, Roger Grosse, and David Duvenaud. Isolating sources of disentanglement in variational autoencoders. *arXiv preprint arXiv:1802.04942*, 2018.

[Do and Tran(2019)] Kien Do and Truyen Tran. Theory and evaluation metrics for learning disentangled representations. *arXiv preprint arXiv:1908.09961*, 2019.

[Eastwood and Williams(2018)] Cian Eastwood and Christopher KI Williams. A framework for the quantitative evaluation of disentangled representations. In *International Conference on Learning Representations*, 2018.

[Eslami et al.(2018)] Eslami, Rezende, Besse, Viola, Morcos, Garnelo, Ruderman, Rusu, Daniilidis, and Zisserman] SM Ali Eslami, Danilo Jimenez Rezende, Frederic Besse, Fabio Viola, Ari S Morcos, Marta Garnelo, Avraham Ruderman, Andrei A Rusu, Ivo Danihelka, Karol Gregor, et al. Neural scene representation and rendering. *Science*, 360(6394):1204–1210, 2018.

[Higgins et al.(2017)] Higgins, Matthey, Pal, Burgess, Glorot, Botvinick, Mohamed, and Lerchner] Irina Higgins, Loic Matthey, Arka Pal, Christopher Burgess, Xavier Glorot, Matthew Botvinick, Shakir Mohamed, and Alexander Lerchner. beta-vae: Learning basic visual concepts with a constrained variational framework. *Iclr*, 2(5):6, 2017.

[Higgins et al.(2018a)] Higgins, Amos, Pfau, Racaniere, Matthey, Rezende, and Lerchner] Irina Higgins, David Amos, David Pfau, Sebastien Racaniere, Loic Matthey, Danilo Rezende, and Alexander Lerchner. Towards a definition of disentangled representations. *arXiv preprint arXiv:1812.02230*, 2018a.

[Higgins et al.(2018b)] Higgins, Amos, Pfau, Racaniere, Matthey, Rezende, and Lerchner] Irina Higgins, David Amos, David Pfau, Sebastien Racaniere, Loic Matthey, Danilo Rezende, and Alexander Lerchner. Towards a definition of disentangled representations. *arXiv preprint arXiv:1812.02230*, 2018b.

[Higgins et al.(2021)] Higgins, Chang, Langston, Hassabis, Summerfield, Tsao, and Botvinick] Irina Higgins, Le Chang, Victoria Langston, Demis Hassabis, Christopher Summerfield, Doris Tsao, and Matthew Botvinick. Unsupervised deep learning identifies semantic disentanglement in single inferotemporal face patch neurons. *Nature communications*, 12(1):1–14, 2021.

[Ioffe and Szegedy(2015)] Sergey Ioffe and Christian Szegedy. Batch normalization: Accelerating deep network training by reducing internal covariate shift. In *International Conference on Machine Learning*, pages 448–456, 2015.

[Iten et al.(2020)] Iten, Metger, Wilming, Del Rio, and Renner] Raban Iten, Tony Metger, Henrik Wilming, Lídia Del Rio, and Renato Renner. Discovering physical concepts with neural networks. *Physical review letters*, 124(1):010508, 2020.

[Kim and Mnih(2018)] Hyunjik Kim and Andriy Mnih. Disentangling by factorising. In *International Conference on Machine Learning*, pages 2649–2658. PMLR, 2018.

[Kingma and Welling(2013)] Diederik P Kingma and Max Welling. Auto-encoding variational bayes. *arXiv preprint arXiv:1312.6114*, 2013.

[Liu et al.(2015)] Liu, Luo, Wang, and Tang] Ziwei Liu, Ping Luo, Xiaogang Wang, and Xiaoou Tang. Deep learning face attributes in the wild. In *Proceedings of International Conference on Computer Vision (ICCV)*, December 2015.

[Locatello et al.(2019)] Locatello, Tschannen, Bauer, Rätsch, Schölkopf, and Bachem] Francesco Locatello, Michael Tschannen, Stefan Bauer, Gunnar Rätsch, Bernhard Schölkopf, and Olivier Bachem. Disentangling factors of variation using few labels. *arXiv preprint arXiv:1905.01258*, 2019.

[Matthey et al.(2017)] Matthey, Higgins, Hassabis, and Lerchner] Loic Matthey, Irina Higgins, Demis Hassabis, and Alexander Lerchner. dsprites: Disentanglement testing sprites dataset. <https://github.com/deepmind/dsprites-dataset/>, 2017.

[Pan et al.(2020)] Pan, Dai, Liu, Loy, and Luo] Xingang Pan, Bo Dai, Ziwei Liu, Chen Change Loy, and Ping Luo. Do 2d gans know 3d shape? unsupervised 3d shape reconstruction from 2d image gans. *arXiv preprint arXiv:2011.00844*, 2020.

[Paysan et al.(2009)] Paysan, Knothe, Amberg, Romdhani, and Vetter] Pascal Paysan, Reinhard Knothe, Brian Amberg, Sami Romdhani, and Thomas Vetter. A 3d face model for pose and illumination invariant face recognition. In *2009 sixth IEEE international conference on advanced video and signal based surveillance*, pages 296–301. Ieee, 2009.

[Rezende and Mohamed(2015)] Danilo Rezende and Shakir Mohamed. Variational inference with normalizing flows. In *International Conference on Machine Learning*, pages 1530–1538, 2015.

[Ridgeway(2016)] Karl Ridgeway. A survey of inductive biases for factorial representation-learning. *arXiv preprint arXiv:1612.05299*, 2016.

[Ridgeway and Mozer(2018)] Karl Ridgeway and Michael C Mozer. Learning deep disentangled embeddings with the f-statistic loss. *arXiv preprint arXiv:1802.05312*, 2018.

[Rudin et al.(2022)] Rudin, Chen, Chen, Huang, Semenova, and Zhong] Cynthia Rudin, Chaofan Chen, Zhi Chen, Haiyang Huang, Lesia Semenova, and Chudi Zhong. Interpretable machine learning: Fundamental principles and 10 grand challenges. *Statistics Surveys*, 16: 1–85, 2022.

[Sepliarskaia et al.(2019)] Sepliarskaia, Kiseleva, de Rijke, et al.] Anna Sepliarskaia, Julia Kiseleva, Maarten de Rijke, et al. Evaluating disentangled representations. *arXiv preprint arXiv:1910.05587*, 2019.

[Takahashi et al.(2019)] Takahashi, Iwata, Yamanaka, Yamada, and Yagi] Hiroshi Takahashi, Tomoharu Iwata, Yuki Yamanaka, Masanori Yamada, and Satoshi Yagi. Variational autoencoder with implicit optimal priors. *Proceedings of the AAAI Conference on Artificial Intelligence*, 33(01): 5066–5073, 2019.

[Tolstikhin et al.(2018)] Tolstikhin, Bousquet, Gelly, and Schölkopf] I Tolstikhin, O Bousquet, S Gelly, and B Schölkopf. Wasserstein auto-encoders. In *International Conference on Learning Representations (ICLR 2018)*. OpenReview. net, 2018.

[Tomczak and Welling(2018)] Jakub Tomczak and Max Welling. Vae with a vampprior. In *International Conference on Artificial Intelligence and Statistics*, pages 1214–1223. PMLR, 2018.

[Tschannen et al.(2018)] Tschannen, Bachem, and Lucic] Michael Tschannen, Olivier Bachem, and Mario Lucic. Recent advances in autoencoder-based representation learning. *arXiv preprint arXiv:1812.05069*, 2018.

[Van Steenkiste et al.(2019)] Van Steenkiste, Locatello, Schmidhuber, and Bachem] Sjoerd Van Steenkiste, Francesco Locatello, Jürgen Schmidhuber, and Olivier Bachem. Are disentangled representations helpful for abstract visual reasoning? *arXiv preprint arXiv:1905.12506*, 2019.

[Yue et al.(2021)] Yue, Wang, Sun, Hua, and Zhang] Zhongqi Yue, Tan Wang, Qianru Sun, Xian-Sheng Hua, and Hanwang Zhang. Counterfactual zero-shot and open-set visual recognition. In *Proceedings of the IEEE/CVF Conference on Computer Vision and Pattern Recognition*, pages 15404–15414, 2021.

[Zaidi et al.(2020)] Zaidi, Boilard, Gagnon, and Carboneau] Julian Zaidi, Jonathan Boilard, Ghyslain Gagnon, and Marc-André Carboneau. Measuring disentanglement: A review of metrics. *arXiv preprint arXiv:2012.09276*, 2020.

[Zhao et al.(2019)] Zhao, Song, and Ermon] Shengjia Zhao, Jiaming Song, and Stefano Ermon. Infovae: Balancing learning and inference in variational autoencoders. In *Proceedings of the AAAI Conference on Artificial Intelligence*, volume 33, pages 5885–5892, 2019.

## APPENDIX

TABLE VIII  
DISENTANGLEMENT SCORES FOR 3D SHAPE DATASET

**Algorithm 1:** Obtaining  $W$  using PCA

**Input:**  $X$ : the entire dataset and  $\alpha$ : hyperparameter less than 1  
**Output:**  $W = [w_1, w_2, \dots, w_n]$   
 $S = [s_1, s_2, \dots, s_n]$ : singular values from  $\text{PCA}(X)$   
 $\bar{S} = [\bar{s}_1, \bar{s}_2, \dots, \bar{s}_n] = S/\max(S)$   
 $W = [w_1, w_2, \dots, w_n]$ : round to 1 decimal place of  $\bar{S}$   
If there exists  $i$  such that  $w_i < 1$ , then  $w_i = \alpha$

**Algorithm 2:** Interpolation layer

**Input:**  $x$  over a mini-batch:  $B = \{x_1, \dots, x_m\}$ .  
**Output:**  $\{y_i = I(x_i)\}$   
 $w_i^k = \min_{j \in \{1, \dots, m\}} d(x_i^k, x_j^k)$  where  
 $x_i = (x_i^k)_{k=1, \dots, n}$   
 $y_i^k = x_i^k + w_i^k * \varepsilon \equiv S(x)$  where  $\varepsilon \sim \mathcal{N}(0, 1)$

TABLE VI  
DISENTANGLEMENT SCORES FOR THE  $XYC$  DATASET

Models / Metrics	z-diff	z-var	dci-rf	jemmig	dcimig
DAE	<b>1.00</b>	<b>1.00</b>	<b>0.99</b>	<b>0.91</b>	<b>0.91</b>
VAE	<b>1.00</b>	0.70	0.14	0.24	0.16
$\beta$ -VAE	<b>1.00</b>	<b>1.00</b>	0.83	0.58	0.52
$\beta$ -TCVAE	<b>1.00</b>	<b>1.00</b>	0.94	0.78	0.77
CCI-VAE	<b>1.00</b>	<b>1.00</b>	0.91	0.66	0.62
FVAE	<b>1.00</b>	<b>1.00</b>	0.27	0.34	0.20
InfoVAE	<b>1.00</b>	0.67	0.25	0.29	0.21
WAE	<b>1.00</b>	0.77	0.21	0.28	0.14

TABLE VII  
DISENTANGLEMENT SCORES FOR THE  $XYs$  DATASET

Models / Metrics	z-diff	z-var	dci-rf	jemmig	dcimig
DAE	<b>1.00</b>	<b>1.00</b>	<b>0.98</b>	<b>0.85</b>	<b>0.86</b>
VAE	<b>1.00</b>	0.78	0.37	0.37	0.33
$\beta$ -VAE	<b>1.00</b>	<b>1.00</b>	0.96	0.69	0.65
$\beta$ -TCVAE	<b>1.00</b>	<b>1.00</b>	0.97	0.83	0.80
CCI-VAE	<b>1.00</b>	<b>1.00</b>	0.91	0.68	0.65
FVAE	<b>1.00</b>	0.85	0.48	0.46	0.39
InfoVAE	<b>1.00</b>	0.68	0.28	0.31	0.28
WAE	0.99	0.46	0.10	0.24	0.15

### A. System and Model Configurations

All of our experiments were run on a single hardware consisting two DGX2 nodes, collectively consisting of 32-V100 GPUs, 1.5GB GPU RAM, and 3TB System RAM. Encoder and decoder architecture are the same in all experiments. Encoder has two convolutional layers followed by Batch Normalization layer and LeakyReLU activation. After convolutional layers, there is one fully-connected layer with 64 nodes and another layer which maps to the latent space. The decode part is

Models / Metrics	z-diff	z-var	dci-rf	jemmig	dcimig
DAE	<b>1.00</b>	0.96	0.90	0.74	0.73
VAE	0.96	0.59	0.36	0.26	0.22
$\beta$ -VAE	<b>1.00</b>	<b>1.00</b>	0.91	0.70	0.68
$\beta$ -TCVAE	<b>1.00</b>	0.85	0.78	0.61	0.63
CCI-VAE	0.98	0.89	0.74	0.59	0.59
FVAE	<b>1.00</b>	<b>1.00</b>	<b>0.97</b>	<b>0.82</b>	<b>0.81</b>
InfoVAE	0.99	0.73	0.33	0.23	0.20
WAE	0.93	0.43	0.13	0.12	0.06

TABLE IX  
DISENTANGLEMENT SCORES FOR 3D FACE MODEL DATASET

Models / Metrics	z-diff	z-var	dci-rf	jemmig	dcimig
DAE	<b>1.00</b>	0.82	0.57	0.46	<b>0.44</b>
VAE	<b>1.00</b>	0.66	0.48	0.38	0.23
$\beta$ -VAE	<b>1.00</b>	0.74	<b>0.68</b>	0.48	0.36
$\beta$ -TCVAE	<b>1.00</b>	<b>0.83</b>	0.65	<b>0.54</b>	<b>0.44</b>
CCI-VAE	<b>1.00</b>	<b>0.83</b>	0.61	0.47	0.34
FVAE	<b>1.00</b>	0.65	0.48	0.37	0.21
InfoVAE	<b>1.00</b>	0.79	0.58	0.47	0.29
WAE	<b>1.00</b>	0.75	0.21	0.26	0.16

symmetric to the encoder part.  $C$  for CCI-VAE is set as 25 for all experiments. We will make all codes public in the future.

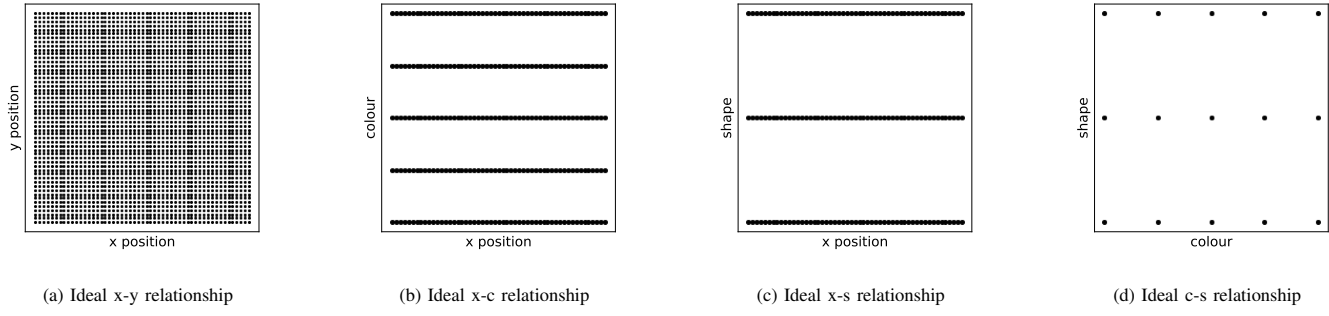


Fig. 5. Ideal relationships between x-y, x-c, x-s and c-s components.

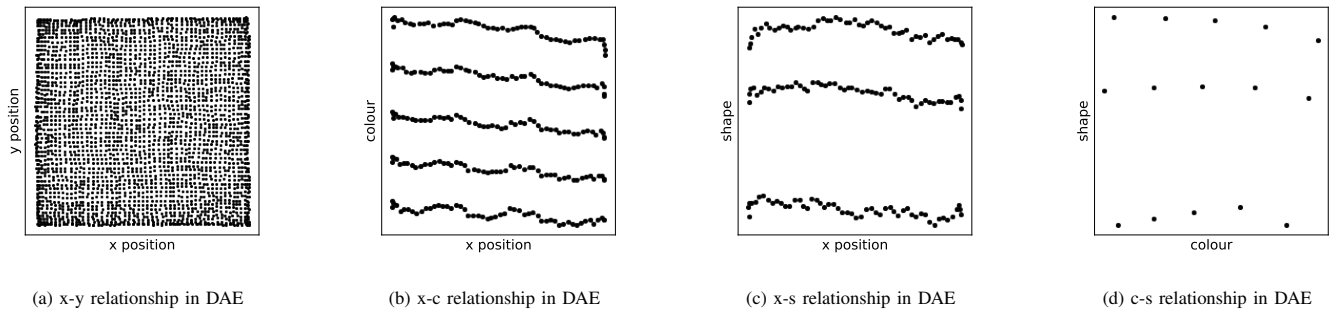


Fig. 6. Relationships between x-y, x-c, x-s and c-s components in DAE.

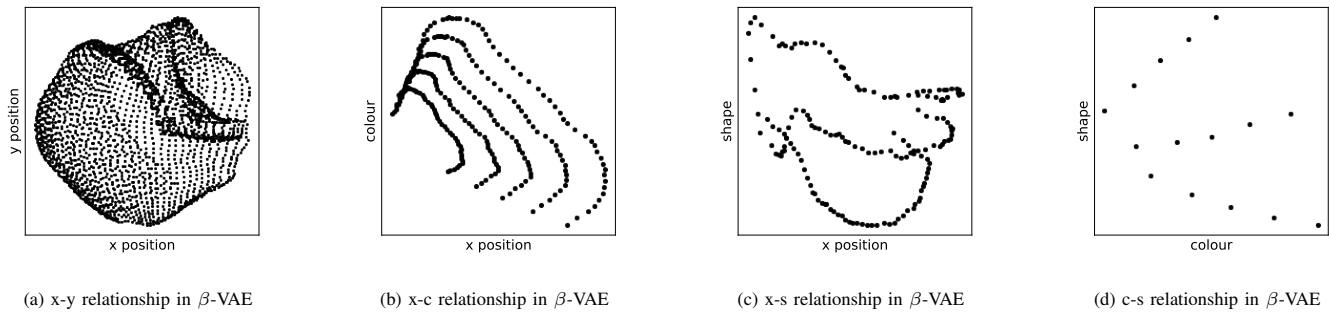


Fig. 7. Relationships between x-y, x-c, x-s and c-s components in  $\beta$ -VAE.

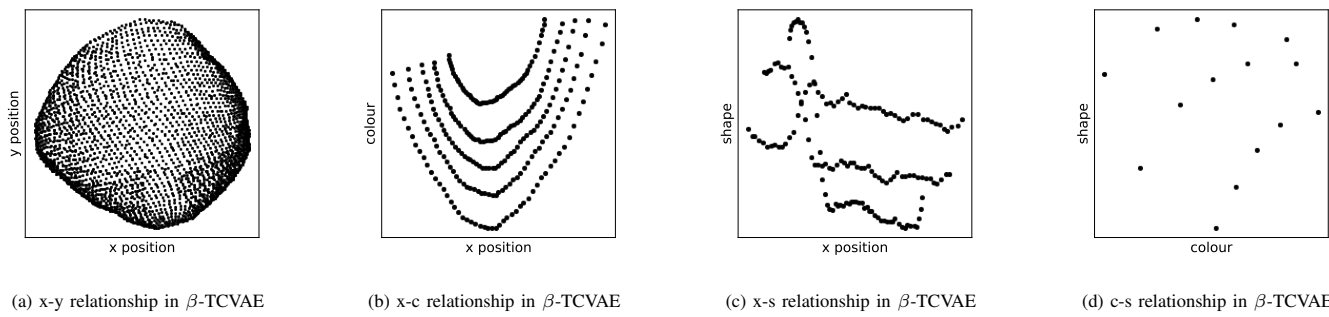
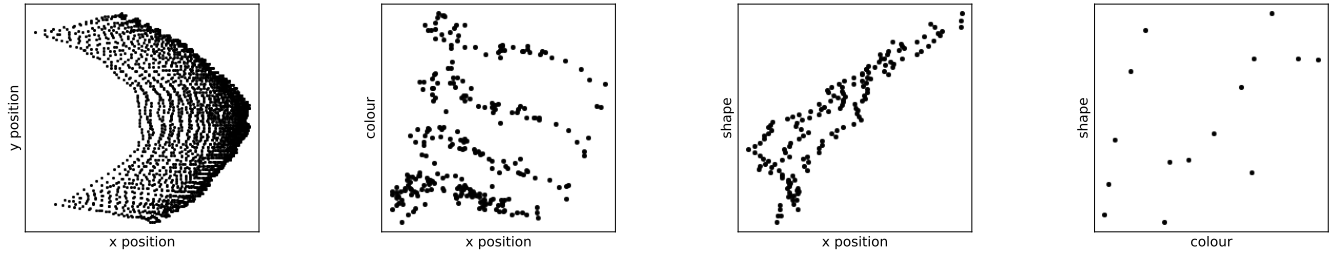


Fig. 8. Relationships between x-y, x-c, x-s and c-s components in  $\beta$ -TCVAE.



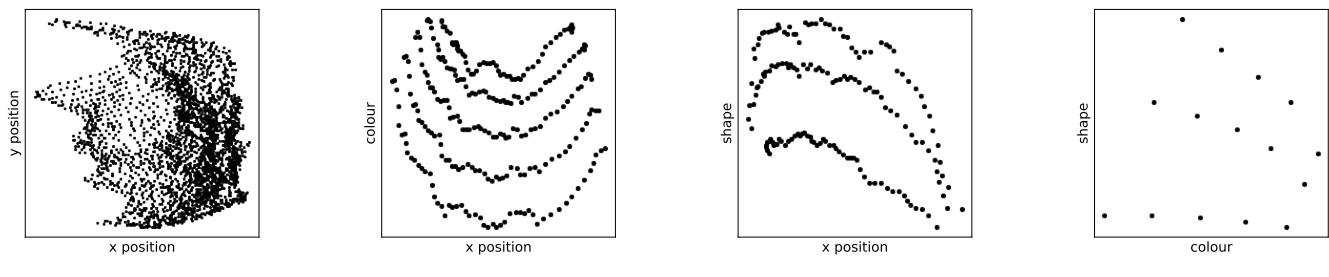
(a) x-y relationship in CCI-VAE

(b) x-c relationship in CCI-VAE

(c) x-s relationship in CCI-VAE

(d) c-s relationship in CCI-VAE

Fig. 9. Relationships between x-y, x-c, x-s and c-s components in CCI-VAE.



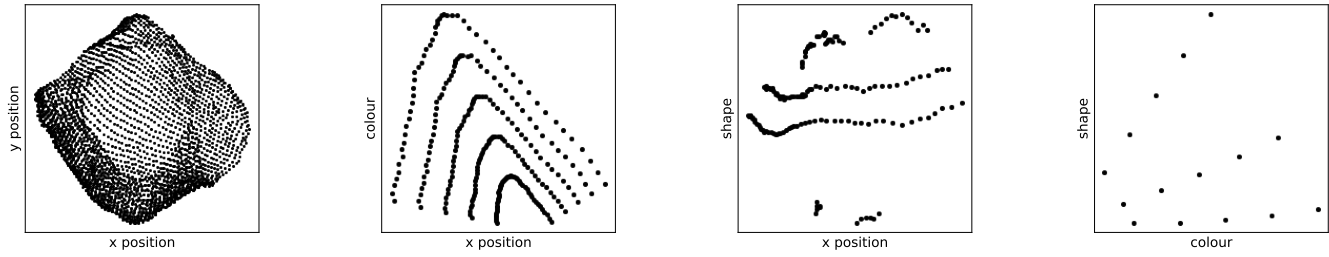
(a) x-y relationship in FVAE

(b) x-c relationship in FVAE

(c) x-s relationship in FVAE

(d) c-s relationship in FVAE

Fig. 10. Relationships between x-y, x-c, x-s and c-s components in FVAE.



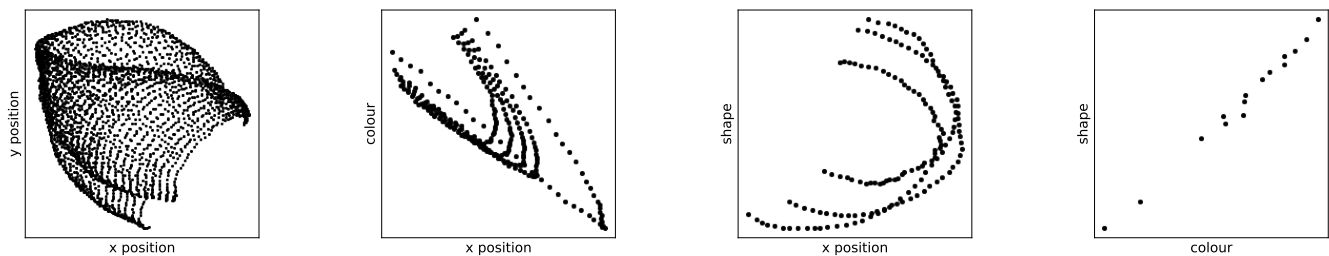
(a) x-y relationship in InfoVAE

(b) x-c relationship in InfoVAE

(c) x-s relationship in InfoVAE

(d) c-s relationship in InfoVAE

Fig. 11. Relationships between x-y, x-c, x-s and c-s components in InfoVAE.



(a) x-y relationship in VAE

(b) x-c relationship in VAE

(c) x-s relationship in VAE

(d) c-s relationship in VAE

Fig. 12. Relationships between x-y, x-c, x-s and c-s components in VAE.

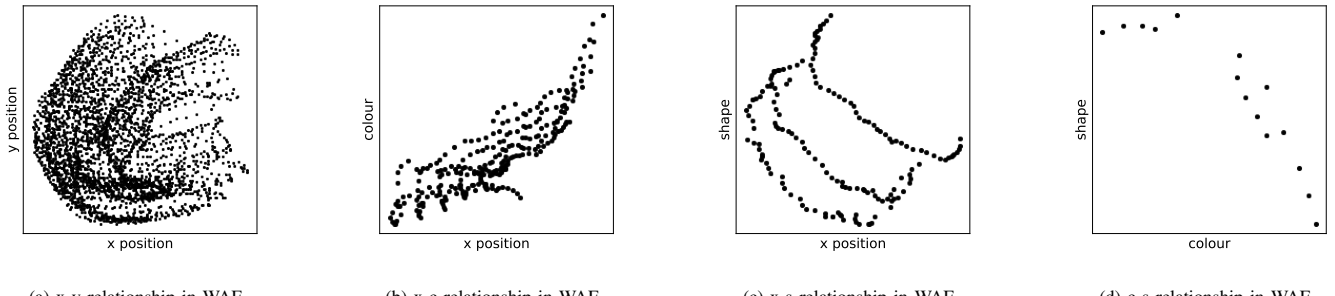


Fig. 13. Relationships between x-y, x-c, x-s and c-s components in WAE.

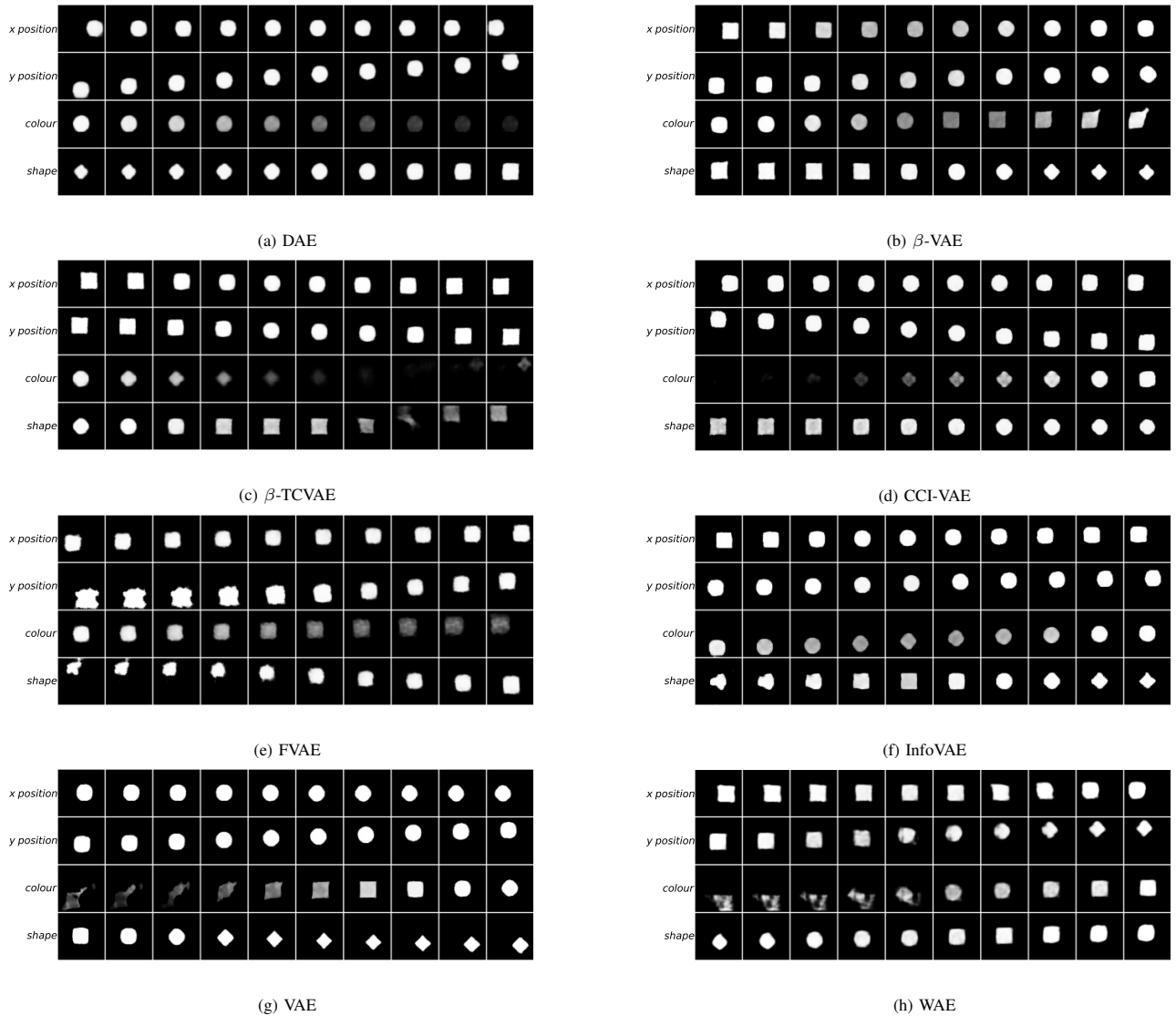


Fig. 14. Reconstructions of latent traversals across each latent dimension in the XYCS dataset.

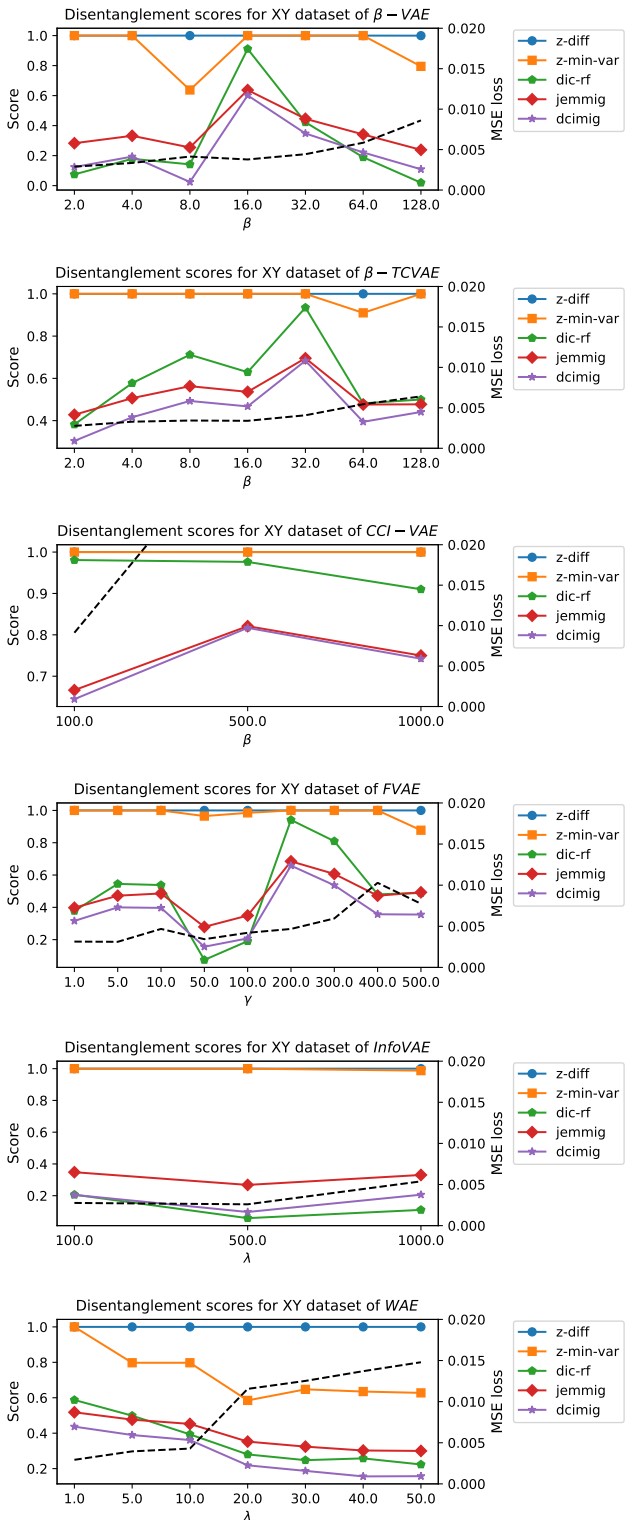


Fig. 15. Disentanglement scores with XY dataset with respect to hyperparameters.

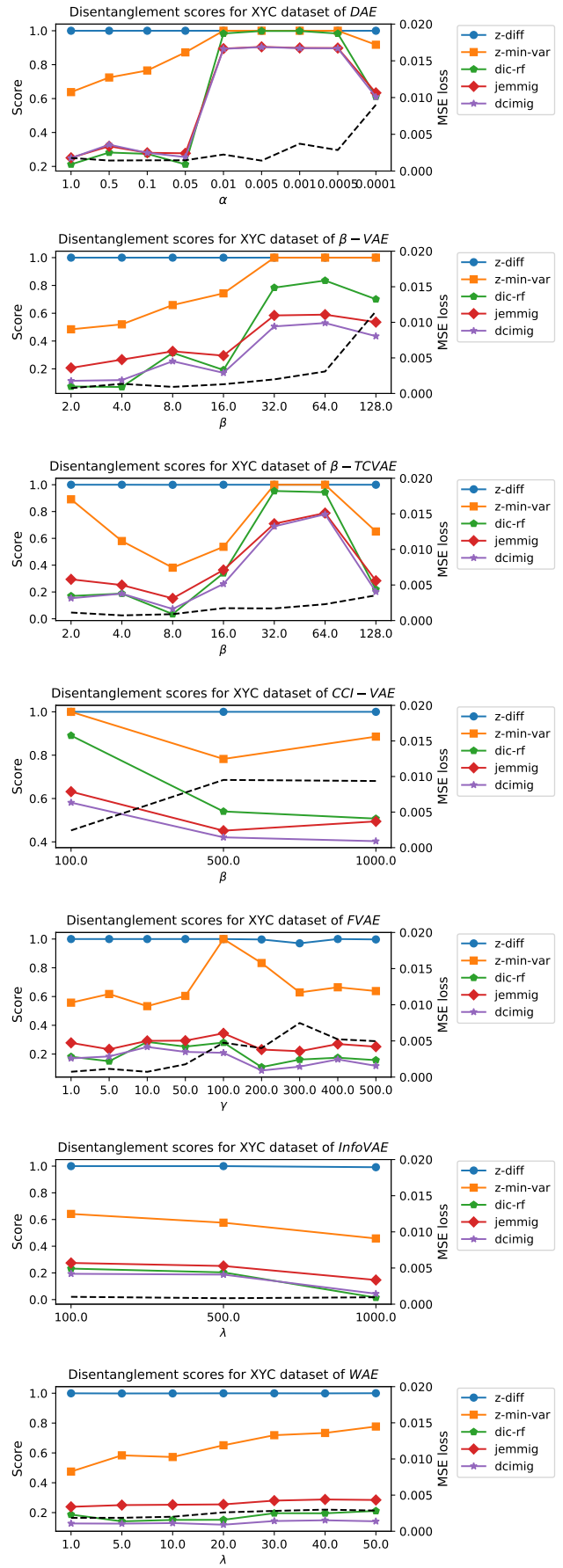


Fig. 16. Disentanglement scores with XYC dataset with respect to hyperparameters.

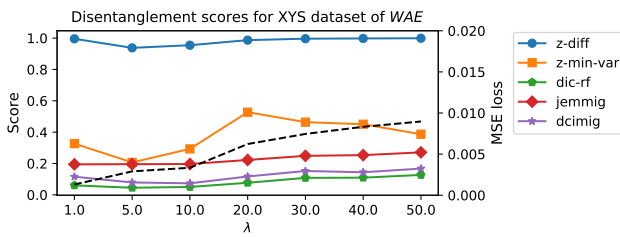
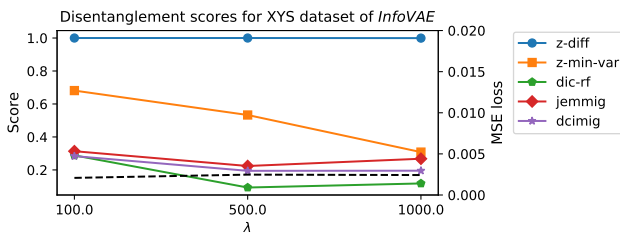
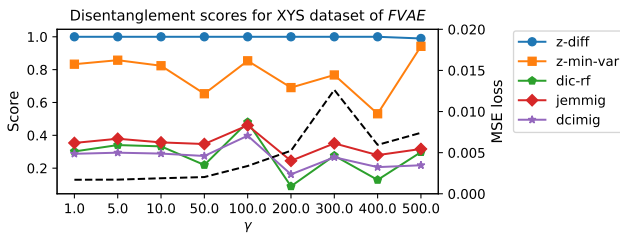
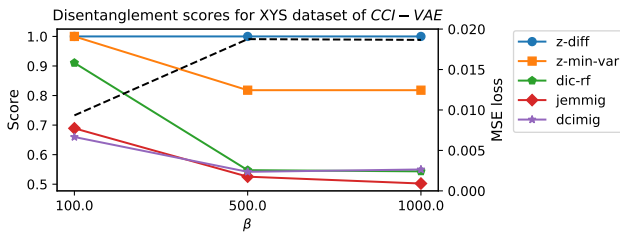
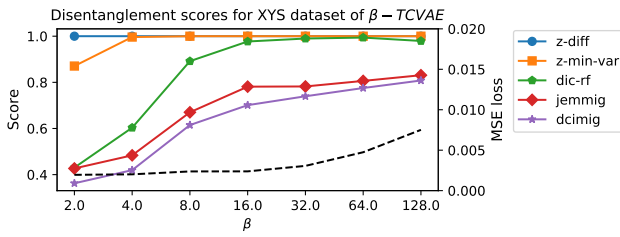
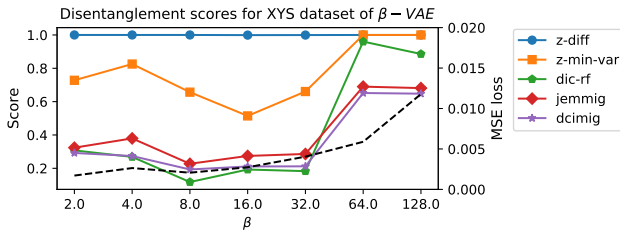
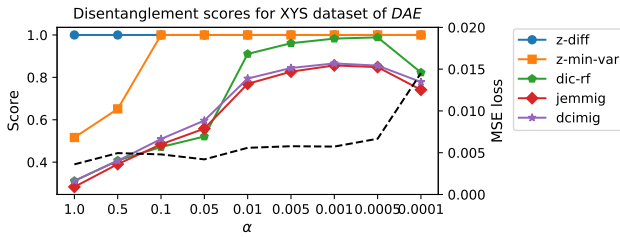


Fig. 17. Disentanglement scores with XYS dataset with respect to hyperparameters.

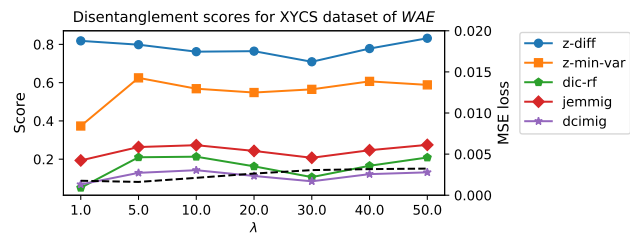
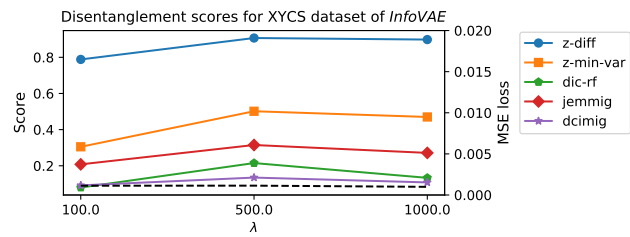
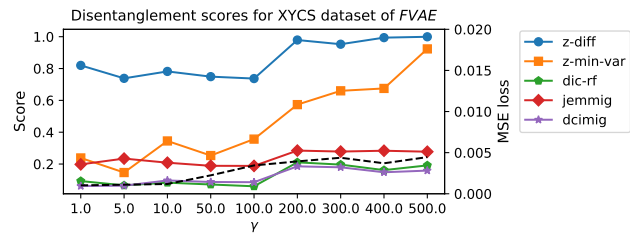
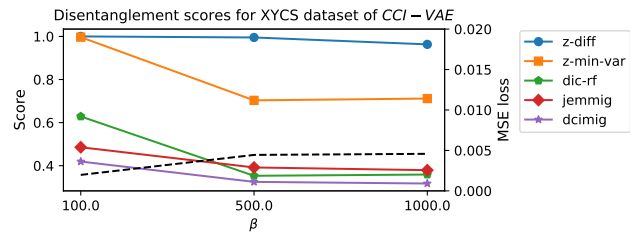
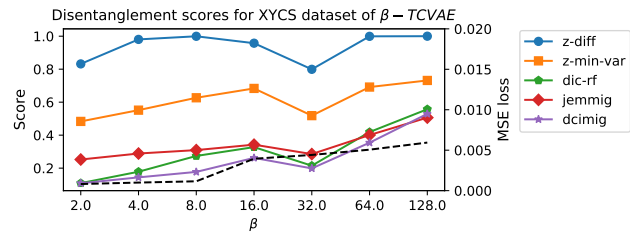
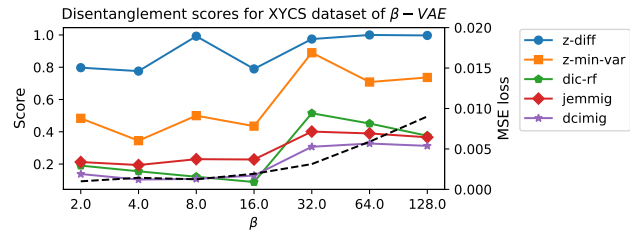
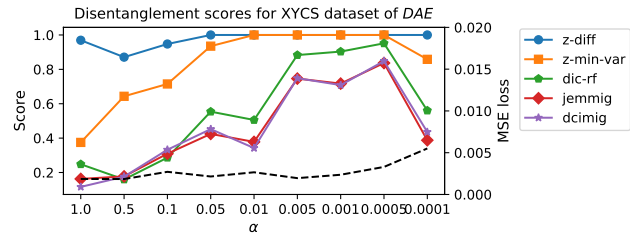
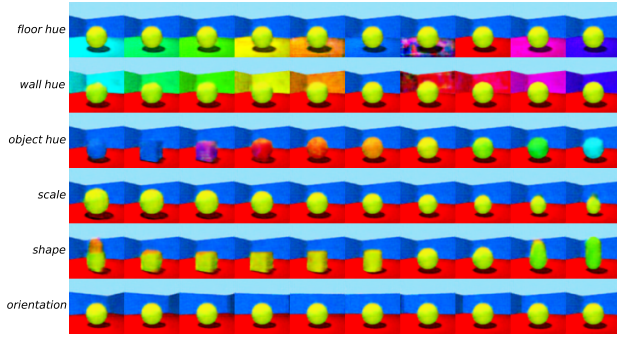
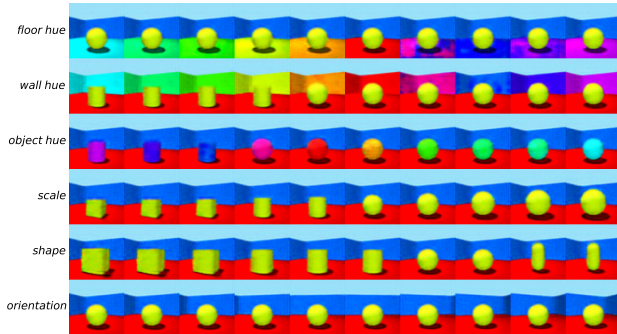


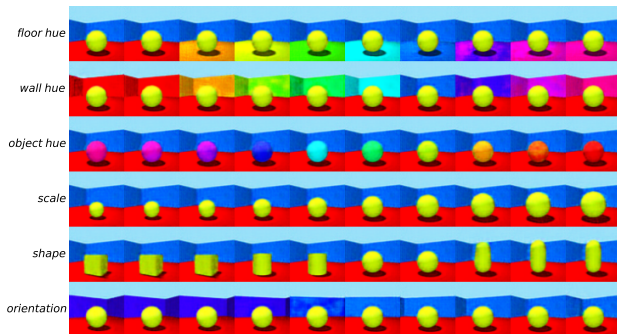
Fig. 18. Disentanglement scores with XYCS dataset with respect to hyperparameters.



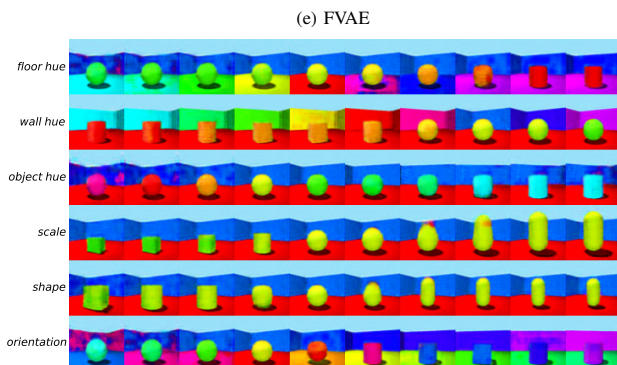
(a) DAE



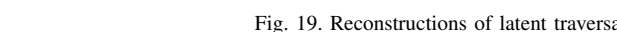
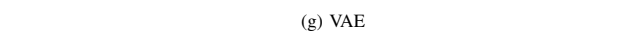
(b)  $\beta$ -VAE



(c)  $\beta$ -TCVAE



(d) CCI-VAE



(e) FVAE



(f) InfoVAE



(g) VAE



(h) WAE

Fig. 19. Reconstructions of latent traversals across each latent dimension in the 3D shape dataset.



(a) DAE



(b)  $\beta$ -VAE



(c)  $\beta$ -TCVAE



(d) CCI-VAE



(e) FVAE



(f) InfoVAE



(g) VAE

Fig. 20. Reconstructions of latent traversals across each latent dimension in the 3D Face Model dataset. We do not visualize the result of WAE since the model fails to disentangle the data.